

Effect of the confinement on two-dimensional complex plasmas with the shear force

Haoyu Qi(齐颢与), Yang Liu(刘阳), Shaohuang Bian(卞少皇), Runing Liang(梁儒宁), Dan Zhang(张丹), and Feng Huang(黄峰)

Citation: Chin. Phys. B, 2025, 34 (**10**): 105203. DOI: 10.1088/1674-1056/adf17c
http://cpb.iphy.ac.cn; http://iopscience.iop.org/cpb

What follows is a list of articles you may be interested in

Diagnosis of electron temperature of copper foil plasmas produced at the Shenguang-II facility

Chenglong Zhang(张成龙), Haochen Gu(谷昊琛), Yu Dai(戴羽), Ke Fang(方可), Yufeng Dong(董玉峰), Peng Zhou(周鹏), and Yingjun Li(李英骏)

Chin. Phys. B, 2025, 34 (**7**): 075202. DOI: 10.1088/1674-1056/adca19

Influence of crystal dimension on performance of spherical crystal self-emission imager

Chenglong Zhang(张成龙), Yihang Zhang(张翌航), Haochen Gu(谷昊琛), Nuo Chen(陈诺), Xiaohui Yuan(远晓辉), Zhe Zhang(张喆), Miaohua Xu(徐妙华), Yutong Li(李玉同), Yingjun Li(李英骏), and Jie Zhang(张杰)

Chin. Phys. B, 2024, 33 (**12**): 125205. DOI: 10.1088/1674-1056/ad84d2

Global dust density in two-dimensional complex plasma

Yi-Zhen Zhao(赵逸真), Song-Fen Liu(刘松芬), Wei Kong(孔伟), and Fang Yang(杨芳)

Chin. Phys. B, 2024, 33 (**6**): 065201. DOI: 10.1088/1674-1056/ad2a76

Simulation of deuterium pellet ablation and deposition in the EAST tokamak with HPI2 code

Da-Zheng Li(李大正), Jie Zhang(张洁), Ji-Lei Hou(侯吉磊), Mao Li(李懋), and Ji-Zhong Sun(孙继忠)

Chin. Phys. B, 2024, 33 (**4**): 045204. DOI: 10.1088/1674-1056/ad1e68

Error field penetration in J-TEXT tokamak based on two-fluid drift-MHD model

Wen Wang(王文), Tao Xu(徐涛), Yi Zhang(张仪), and the J-TEXT team

Chin. Phys. B, 2024, 33 (**4**): 045202. DOI: 10.1088/1674-1056/ad1e6b

---

Effect of the confinement on two-dimensional complex plasmas with the shear force

Haoyu Qi(齐颢与)[1,2,†], Yang Liu(刘阳)[1,3,†], Shaohuang Bian(卞少皇)[4], Runing Liang(梁儒宁)[1], Dan Zhang(张丹)[1], and Feng Huang(黄峰)[1,‡]

[1] *College of Science, China Agricultural University, Beijing* 100083, *China*
[2] *Office for Science and Technology, Northwest University, Xi'an* 710069, *China*
[3] *Institut für Experimentelle und Angewandte Physik, Christian-Albrechts-Universität, D-*24098 *Kiel, Germany*
[4] *College of Information and Electrical Engineering, China Agricultural University, Beijing* 100083, *China*

(Received 26 February 2025; revised manuscript received 4 July 2025; accepted manuscript online 18 July 2025)

Langevin molecular dynamics simulations reveal the impact of confinement strength on the structure and dynamics of a two-dimensional complex plasma under constant shear force. Structural analysis via Voronoi diagrams and the local bond-order parameter $|\Psi_6|$ shows that stronger confinement enhances hexagonal order and mitigates shear-induced disorder. Dynamical properties, determined by mean-square displacement (MSD) and the velocity autocorrelation function (VACF), indicate that the shear-induced superdiffusion weakens with increasing confinement strength. The entropy change (ΔS) shows that strong confinement ($\omega > 1$) balances particle dynamics between shear and shear-free regions, thereby stabilizing the system. These findings highlight the interplay between confinement and shear force.

Keywords: complex plasmas, steady shear flow, Langevin dynamics simulation, confinement

PACS: 52.27.Lw, 83.50.Ax, 05.10.Gg, 52.58.Qv

DOI: 10.1088/1674-1056/adf17c **CSTR:** 32038.14.CPB.adf17c

1. Introduction

Two-dimensional (2D) complex plasmas, owing to their tunable interparticle interactions, visual accessibility across spatial and temporal scales, and well-resolved dynamical behavior, have been extensively employed to investigate structural phase transitions and transport processes in strongly coupled systems.[1–3] In these systems, the external confinement potential and the applied shear force are two key factors influencing both microscopic structure and macroscopic behavior. Confinement determines the spatial distribution and boundary morphology of the particle ensemble, while the shear force continuously injects energy into the system, driving structural evolution far from equilibrium.[4,5]

Previous studies have examined the roles of these two factors from different perspectives. For example, Schweigert *et al.*[3] and Quinn and Goree[6] investigated the influence of static confinement on structural transitions and thermodynamic properties in finite dust clusters. Maity *et al.*[5] systematically analyzed the effects of confinement strength on structural ordering and dynamical characteristics. In contrast, Liu and Goree,[4] as well as Nosenko and Goree,[7] focused on nonequilibrium behaviors under shear driving, reporting phenomena such as superdiffusion, spontaneous structural rearrangements, and shear-induced melting.

However, most existing studies have treated external confinement and shear driving as independent factors. Investigations of external confinement typically consider near-static or thermally equilibrated conditions, whereas shear-driven dynamics are often studied under fixed or periodic boundary conditions without accounting for variations in confinement. As a result, the coupled effect between confinement and sustained driving remains poorly understood. In particular, it is unclear how confinement strength modulates structural stability, energy-dissipation pathways, and macroscopic organization in nonequilibrium plasmas.

To address these open questions, we develop a two-dimensional complex plasma model that incorporates both steady directional shear force and spatial confinement. By employing Langevin dynamics, the model explicitly accounts for thermal fluctuations and dissipative processes, enabling accurate simulation of nonequilibrium particle motion. Through systematic variation of the confinement strength, we demonstrate its crucial role in reducing shear-induced distortions and stabilizing microstructure. We further analyze the response of structural metrics, including bond-orientational order and local structural entropy, to shear under varying confinement conditions. This work provides new insight into the interplay between confinement and driving in strongly coupled systems and offers theoretical guidance for controlling transport and structural organization in driven complex plasmas.

[†]These authors contributed equally to this work.
[‡]Corresponding author. E-mail: 05033@cau.edu.cn
© 2025 Chinese Physical Society and IOP Publishing Ltd. All rights, including for text and data mining, AI training, and similar technologies, are reserved.

2. Simulation model

Langevin dynamics simulations are a general approach widely used in many fields, e.g., medical image reconstruction,[8] the diffusion of proteins,[9] non-Gaussian diffusion of cytoplasmic particles under different cell wall confinement conditions,[10] and the dynamic heterogeneity of soft matter.[11] In this paper, we employ Langevin dynamics simulations[12,13] to investigate the influence of system confinement on the structural organization and dynamical stability of complex plasma systems under continuous shear force conditions. The simulation utilizes classical Newtonian mechanics to describe particle motion, incorporating a self-consistent treatment of Brownian motion and damping effects to closely approximate real dusty plasma experiments.[12,13] Accurate particle trajectories are obtained using the velocity Verlet scheme to numerically solve the equation of motion.[14]

The simulation models a two-dimensional complex plasma system consisting of 196 dust particles with identical mass m and charge q, confined by a radial confinement potential. According to previous work,[15] this system size of $N = 196$ is sufficient to reliably capture collective behavior and fluid characteristics. All length scales are normalized by the plasma Debye length λ_{D}. Initially, particles are uniformly distributed within a simulation box of $L \times L$ ($L = 14$). The system has a parabolic potential boundary condition that binds the particles into a cluster, and half of the cluster area is exposed to a directional shear force to study its response. The particle dynamics are governed by the following equation of motion:

$$\boldsymbol{F}_i = \sum_{i \neq j}^{N} \boldsymbol{F}_{ij} + \boldsymbol{F}_{\mathrm{c}i} + \boldsymbol{F}_{\mathrm{ran}} + \boldsymbol{F}_{\mu} + \boldsymbol{f}, \tag{1}$$

where $\boldsymbol{F}_{ij} = -\nabla \Phi_Y$ is the interaction force between particles. The screened Yukawa potential is defined as

$$\Phi_Y = \frac{q^2}{r_{ij}} \left(\mathrm{e}^{-r_{ij}/\lambda_{\mathrm{D}}} - \beta \right),$$

which involves short-range repulsion and long-range attraction. Here, r_{ij} is the distance between particles i and j. The parameter β is the attraction coefficient used to characterize the long-range attractive component of the interparticle potential. In this work, we set $\beta = 0.1$, following previous studies where a similar range was used to investigate structural and dynamical effects of weak long-range attraction in two-dimensional dusty plasmas.[16–18] The attraction term primarily originates from shielding and scattering of the plasma by neighboring dust particles, collective ion oscillations in the plasma sheath, charge–dipole interactions of polarized particles, and the positive background of dusty plasmas.[19,20]

The external radial confinement force is expressed by

$$\boldsymbol{F}_{\mathrm{c}i} = -\nabla \left(\tfrac{1}{2} m \omega^2 r_i^2 \right) = -m\omega^2 \boldsymbol{r}_i, \tag{2}$$

where ω denotes the confinement strength and r_i represents the position of particle i. The harmonic potential is consistent with general dusty plasma experiments. $\boldsymbol{F}_{\mathrm{ran}}$ represents the random (thermal) force, while $\boldsymbol{F}_{\mu} = -m\mu \, \mathrm{d}\boldsymbol{r}/\mathrm{d}t$ is the frictional force with $\mu = 0.02$.[21–24] A directed constant shear force $\boldsymbol{f}$ is applied to the lower half of the cluster ($y < 0$), ensuring continuous energy injection under different confinement strengths. Energy transfer across the interface between sheared and unsheared regions allows half-cluster driving to influence the overall system dynamics. Experimentally, directed shear forces can be realized under both gravity and microgravity conditions through several methods, including laser-induced radiation pressure,[25–27] thermophoretic forces,[28] airflow-generated thrust,[12,13] and ion drag forces, as prominently observed in the PK-3 Plus facility.[29] In this simulation, the shear force is fixed at a dimensionless value of $f = 2$. As concluded in our previous work,[12] this magnitude is sufficient to induce significant dynamical responses in the cluster while maintaining structural integrity and preventing particle escape.

The calculation of normalized parameters follows Ref. [16]. Energy is normalized by $E_0 = q^2/\lambda_{\mathrm{D}}$, and the normalization time $t_0 = \sqrt{m\lambda_{\mathrm{D}}^3/q^2}$ represents the characteristic timescale of particle motion and system response in dusty plasmas.[30,31] This normalization enables consistent comparison of dust systems under different confinement strengths. The cutoff radius is set to 12 to reduce computation time. The simulation time step is $0.02t_0$, and the total run spans 20000 time steps, which is sufficient for the system to reach equilibrium. By varying the confinement strength ω, we analyze how particle configurations and dynamic behavior evolve under a constant shear force.

In this model, the dynamics of electrons and ions are not explicitly introduced. This is because in complex plasmas, the response time of electrons and ions (nanoseconds) are much faster than those of dust particles (milliseconds), and the two timescales are clearly separated. Thus, a quasi-static approximation is adopted: electrons and ions are assumed to be in instantaneous equilibrium, with their collective effects effectively represented by the shielding Yukawa potential. The shielding length λ_{D} is determined by the density and temperature of background electrons and ions, while the long-range attraction term β reflects charge–dipole coupling. This treatment greatly reduces computational complexity while preserving physical consistency.

To illustrate how confinement and shear forces affect the structure of the dusty plasma cluster, a schematic diagram is shown in Fig. 1. Without external shear, particles are confined near the center by a radial electric field, forming a circular cluster in equilibrium. Stronger radial confinement makes the cluster more compact. When an external shear is applied, the force balance is disturbed: the cluster elongates along the

shear direction, and its center of mass shifts from the origin. This schematic provides a conceptual guide to the physical processes explored in our simulations.

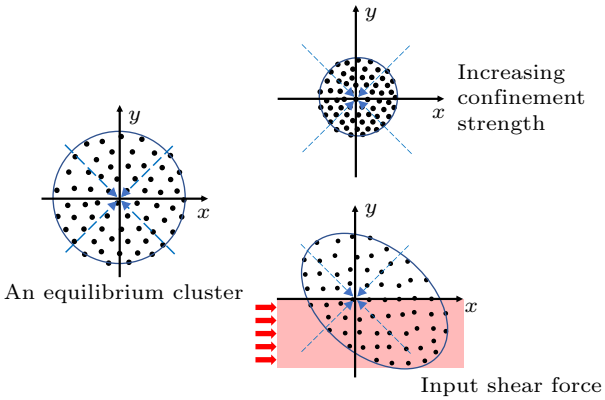


Fig. 1. Schematic diagram of the simulation. The left panel shows a complex plasma cluster in equilibrium under radial confinement without external shear. As the radial confinement increases, the cluster becomes more compact and its size decreases. When a shear force is applied, the circular cluster is stretched along the shear direction, and the cluster center shifts away from the origin.

3. Results and analysis

Figure 2 illustrates the particle distribution under shear force with different external confinement conditions when the system reaches the steady state. From Fig. 2(a1), it can be observed that under weak confinement and continuous local shear (applied only in the lower half region of the cluster, marked in red), the cluster becomes elongated and deviates from its original equilibrium position. The attraction among particles binds them together, preventing diffusion. As the confinement strength ω increases from 0.2 to 5, a denser particle distribution and significant compression of cluster size are observed. Simultaneously, the cluster center gradually returns to its original position due to the strong confinement applied to the entire system. Square boxes of equal size (4×4) are selected at the shear boundaries to study the cluster configuration (marked by the green box in Figs. 2(a1)–2(a3)), and the corresponding Voronoi diagrams are plotted in Fig. 2(b1)–2(b3). The Voronoi diagram partitions space into regions where every point within a region is closer to its associated particle than to any other, with boundaries defined by the perpendicular bisectors of adjacent particle pairs.[32–35] This method is a useful tool for analyzing particle distributions and system ordering. At $\omega = 0.2$, the green region contains only 14 particles that form irregular polygons. As the confinement strength increases to 0.8, 50 particles appear in the green region, mostly forming irregular hexagons. At $\omega = 5$, the green box contains all particles, forming a highly regular hexagonal structure. It can be concluded that stronger confinement enhances the order and weakens the influence of the sustained shear force.

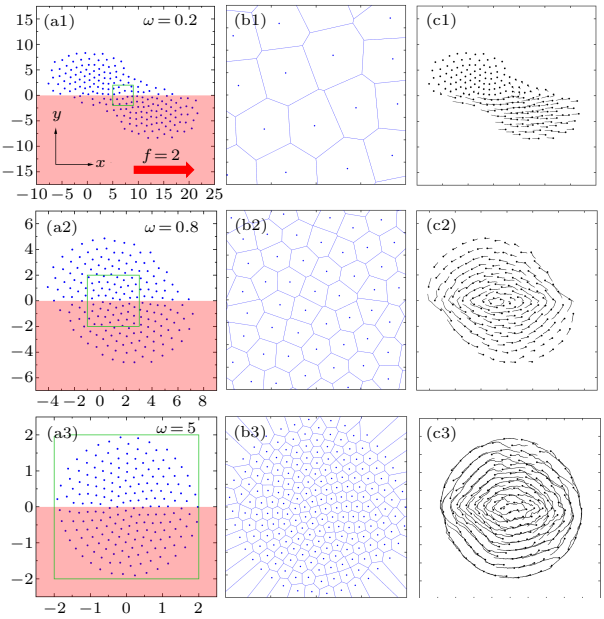


Fig. 2. Steady-state particle distributions under different confinement strengths: (a1) $\omega = 0.2$, (a2) $\omega = 0.8$, and (a3) $\omega = 5$ at $20000t_0$. Corresponding Voronoi diagrams within the green squares are shown in (b1)–(b3), and particle trajectories over 3000 time steps in steady state are shown in (c1)–(c3), corresponding to (a1)–(a3). The green squares, all of size 4×4, are located at the shear boundary.

To illustrate the dynamical response of the cluster at different confinement strengths (in Figs. 2(a1)–2(a3)), the particle trajectories over 3000 time steps in steady state are shown in Figs. 2(c1)–2(c3). These trajectories show the long-time behavior of particles under varying ω while keeping the shear force constant. As shown in Fig. 2(c1), at $\omega = 0.2$, the confinement is weak, and particles in the shear-affected region exhibit significantly enhanced mobility and a pronounced tendency to escape the cluster. This suggests that the external shear force is sufficient to overcome the restoring forces provided by the Yukawa interactions and the external confinement potential, thus compromising the structural integrity of the cluster. As the confinement strength increases to $\omega = 0.8$ and further to $\omega = 5$ (see Figs. 2(c2) and 2(c3)), the distinction between the shear and non-shear regions becomes less pronounced. This indicates that the system gradually approaches a dynamic balance, where the external shear force is balanced by the confinement and interparticle interactions. Under such conditions, particle motion becomes increasingly coherent and organized, leading to the formation of stable vortex-like trajectories. These vortices represent a form of collective motion, wherein the shear-induced local motion is redistributed by the strong confinement, effectively transforming the external driving force into rotational patterns through strong interparticle coupling.

The dependence of structural rearrangements under confinement was analyzed by measuring the probability distribution of the local bond-orientational order (BOO), $|\Psi_6| = |\frac{1}{N_k}\sum_{k=1}^{N_k} \exp(i6\theta_{jk})|$, where N_k is the number of nearest neighbors of particle j and θ_{jk} is the angle of the bond from particle

j to its kth neighboring particle.[36–38] $|\Psi_6|$ ranges from 0 to 1 ($|\Psi_6| = 1$ for a perfect hexagonal lattice) and decreases when the locally ordered structure is deformed. To ensure accurate statistics, $|\Psi_6|$ was calculated only for particles in the central region with complete Voronoi cell structures, excluding edge particles that may have incomplete coordination. The range of $|\Psi_6|$ was divided into multiple subintervals, and the probability distribution was obtained by counting the fraction of particles falling into each subinterval. Figure 3 shows that confinement strongly influences the ordering of the cluster. At $\omega = 5$, $|\Psi_6|$ is concentrated around 0.9, indicating a highly ordered hexagonal lattice structure under strong confinement. When the confinement weakens, the peak of $|\Psi_6|$ gradually shifts leftward, and the peak is located around the middle ($|\Psi_6| = 0.5$) at $\omega = 0.2$, indicating that the ordered structure has been destroyed by the shear force.

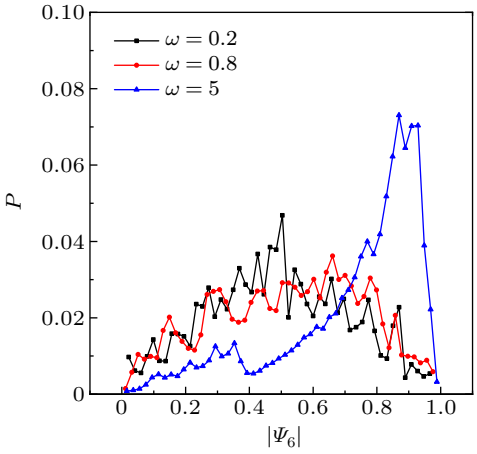


Fig. 3. Probability distribution of the local bond-orientational order parameter $|\Psi_6|$ under different confinement strengths of $\omega = 0.2$, 0.8, and 5.

The dynamical properties of the cluster system are characterized by the mean square displacement (MSD) and the velocity autocorrelation function (VACF), both of which are influenced by the confinement conditions. The MSD of particles is defined as

$$\langle \Delta r^2(t) \rangle = \frac{1}{N} \left\langle \sum_{i=1}^{N} (\boldsymbol{r}_i(t) - \boldsymbol{r}_i(0))^2 \right\rangle, \tag{3}$$

as shown in the log–log plot in Fig. 4(a). The diffusion strength can be quantified by the exponent α from $\langle \Delta r^2(t) \rangle \sim t^{\alpha}$.[39] Normal diffusion corresponds to $\alpha = 1$, while superdiffusion (or enhanced diffusion) occurs at $\alpha > 1$. The dashed line in Fig. 4(a) indicates $\alpha = 1$. It is evident that the slopes of all MSD curves exceed that of the dashed line, especially at longer dynamical timescales, indicating that the constant shear force drives particle trajectories away from regular Brownian motion and gives rise to superdiffusion.[40,41] In contrast, stronger confinement suppresses particle mobility, as reflected in a reduction in MSD with increasing confinement strength.

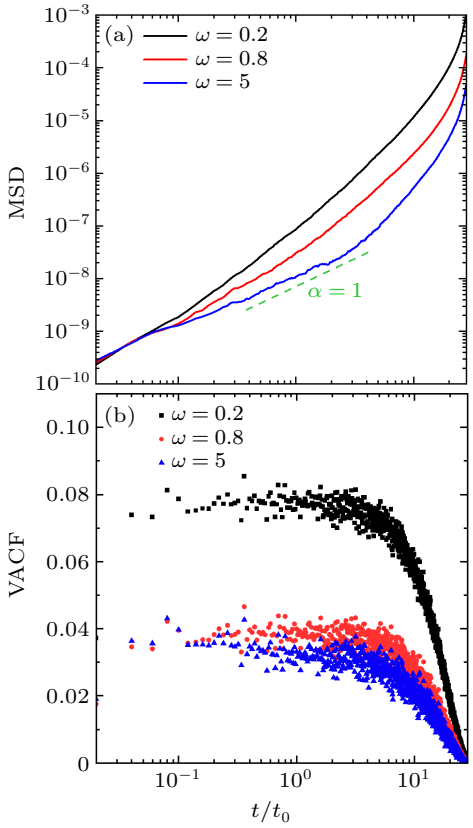


Fig. 4. (a) MSD and (b) VACF of particles under different confinement strengths.

The VACF of the cluster is given by

$$\mathrm{VACF}(t) = \frac{\left\langle \sum_{i=1}^{N} \boldsymbol{v}_i(t) \cdot \boldsymbol{v}_i(0) \right\rangle}{\left\langle \sum_{i=1}^{N} \boldsymbol{v}_i(0) \cdot \boldsymbol{v}_i(0) \right\rangle}, \tag{4}$$

where $\boldsymbol{v}_i(0)$ and $\boldsymbol{v}_i(t)$ denote the velocity of the i-th particle at the moment when the system reaches steady state and at a subsequent time t, respectively. Figure 4(b) shows that with increasing confinement strength, the VACF decreases, indicating weaker correlations in particle motion. Over time, the VACF of all systems eventually approaches zero, implying the loss of velocity correlations at long timescales.

Entropy serves as an effective measure to characterize the thermodynamic properties of strongly coupled systems.[42–45] Popel *et al.*[46] studied the evolution of entropy in plasma systems during the development of modulation processes (i.e., the self-organization associated with the transition from weak to strong turbulence) and the validity of the principle of minimum entropy production. Wong *et al.*[42] showed that complex plasmas under constant shear force also obey the fluctuation theorem. Wieben *et al.*[47] demonstrated that basic thermodynamic principles (i.e., Clausius entropy) remain valid in finite-size complex plasmas. In this paper, we adopt Clausius entropy as a simple criterion to characterize the thermodynamic properties of complex plasmas that can remain in long-term stable states. Clausius entropy[43] is given as

$$S_2 - S_1 = \Delta S = \int_1^2 \frac{\mathrm{d}Q}{T} = C \ln \frac{T_2}{T_1}, \tag{5}$$

where $dQ = C dT$ is the heat transfer of the system and C is the heat capacity. According to the equivalence and ergodicity theorems of classical statistical theory, the heat capacity of a two-dimensional system containing N charged particles follows the Dulong–Petit law, i.e., $C = 2Nk_B$.[47] Here, T_2 and T_1 are the particle temperatures in the shear and shear-free regions, respectively, which are obtained from the kinetic energy E_k of particles. Differences in particle dynamics between regions with and without shear yield the entropy change ΔS, which is strongly dependent on variations in E_k.

Figure 5 shows the entropy change ΔS between shear and shear-free regions. For comparison, we also plot the length difference of the clusters $\Delta W (= L_x - L_y)$, i.e., the difference between the maximum cluster size along the shear direction (L_x) and that in the perpendicular direction (L_y). A perfectly circular cluster corresponds to $\Delta W \approx 0$. From Fig. 5, it is evident that the entropy change ΔS exhibits a strong correlation with ΔW. The influence of ω on ΔS proceeds through three stages: a plateau stage at $\omega < 0.1$, a decay stage at $0.1 < \omega < 1$, and a stabilization stage at $\omega > 1$.

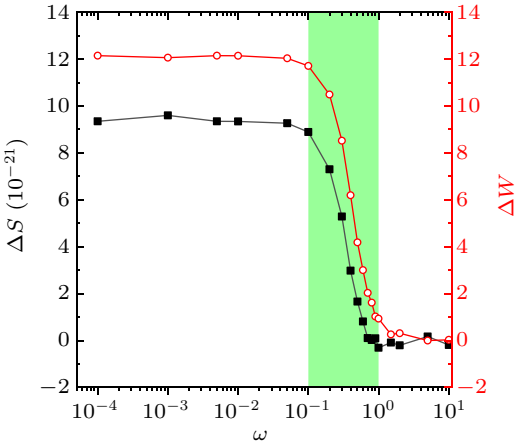


Fig. 5. Entropy change ΔS (black squares) and cluster stretch length difference ΔW (red circles) as functions of the confinement strength ω.

Under extremely weak confinement ($\omega < 0.1$), where radial confinement forces are negligible, shear dominates and induces significant elongation of the cluster along the shear direction (ΔW reaches its maximum). The weak confinement produces loosely bound cluster structures, while the particle dynamics in shear and shear-free regions remain largely decoupled. Consequently, the entropy difference ΔS remains high, reflecting the persistent independence of particle motion between regions. As ω increases (from 0.1 to 1), the elongated cluster gradually relaxes toward a circular shape, which strengthens particle interactions between regions. The denser particle distribution under stronger confinement enhances ordering in the system and drives a reduction in entropy difference. When ω becomes sufficiently strong (> 1), clusters are tightly compressed and highly ordered. Particles are strongly coupled, dynamics between regions become synchronized, and structural fluctuations are suppressed. As a result, the entropy change ΔS stabilizes at a low value, indicating that the shear influence is effectively saturated and further increasing confinement only exerts little additional impact on the system structure.

Figure 6 presents the kinetic energy distributions of particles in the shear and shear-free regions under different confinement strengths ($\omega = 0.2$, 0.3, 0.5, and 5), illustrating the variation in particle dynamics. In Fig. 6(a), when the confinement is weak ($\omega = 0.2$), the particle dynamics in the shear and shear-free regions differ significantly: particles in the shear region acquire much higher kinetic energy, reflecting the strong influence of the shear force. As ω increases (e.g., $\omega = 0.3$ and 0.5), the difference between the kinetic energy distributions of particles in the shear and shear-free regions is gradually decreasing. This indicates that energy transfer occurs between the two regions due to enhanced particle interactions and stronger coupling, thereby reducing the dynamical differences between them (Figs. 6(b) and 6(c)). When the confinement becomes sufficiently strong (e.g., $\omega = 5$), the kinetic energy distributions in the shear and shear-free regions nearly coincide, suggesting that particle dynamics are uniform across regions. In this regime, strong confinement enhances inter-region coupling and suppresses the influence of shear perturbation, consistent with the behavior observed in Fig. 5.

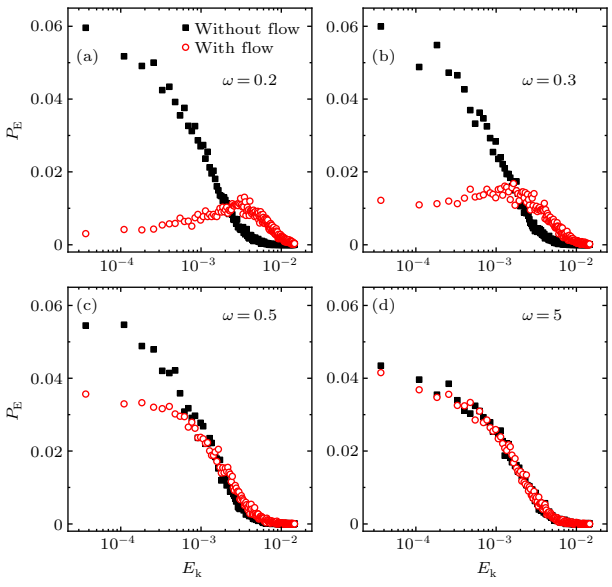


Fig. 6. Kinetic energy distributions P_E of particles in the regions with and without shear force under different confinement strengths of $\omega = 0.2$, 0.3, 0.5, and 5.

4. Summary

In a complex plasma system subjected to a constant shear force, we conduct an in-depth study of how radial confinement enhances structural order and dynamical stability. Our results show that continuous energy input from the shear force signif-

icantly affects the cluster structure, inducing internal disorder and weakening particle coupling. Particles in the shear region exhibit markedly different dynamics compared to those in the non-shear region. This disparity manifests not only in particle velocities and spatial distributions but also in overall system stability and evolution.

Radial confinement effectively mitigates shear-induced disturbances, enhancing interparticle coupling. Under confinement, particles maintain a degree of organized structure even under perturbations, facilitating structural rearrangements. Cluster compression amplifies interparticle forces, enhancing local order and promoting a rebalancing of particle dynamics across the system, resulting in the stable state.

In complex plasmas, particle interactions are influenced not only by shear force but also by local temperature, density, and external boundary conditions. These factors collectively shape system dynamics. Our study provides a paradigm for investigating structural rearrangements and collective dynamics in shear-driven systems, highlighting the role of boundary coupling in mitigating perturbations.

Acknowledgment

Project supported by the National Natural Science Foundation of China (Grant No. 12075315).

References

[1] Maity S and Arora G 2022 *Sci. Rep.* **12** 20430
[2] Vaulina O, Khrapak S and Morfill G 2002 *Phys. Rev. E* **66** 016404
[3] Schweigert V A, Schweigert I V, Melzer A, Homann A and Piel A 1998 *Phys. Rev. Lett.* **80** 5345
[4] Liu B and Goree J 2008 *Phys. Rev. Lett.* **100** 055003
[5] Maity S, Das A, Kumar S and Tiwari S K 2018 *Phys. Plasmas* **25** 043701
[6] Quinn R A and Goree J 2000 *Phys. Rev. E* **61** 3033
[7] Nosenko V and Goree J 2004 *Phys. Rev. Lett.* **93** 155004
[8] Huang J, Wu Q, Ren Y, Yang F, Yang A, Yang Q and Pu X 2024 *Proc. AAAI Conf. Artif. Intell.* **38** 2339
[9] Di Cairano L, Stamm B and Calandrini V 2021 *Biophys. J.* **120** 4722
[10] Yu S, Wu J, Meng X, Chu R, Li X and Wu G 2021 *Entropy* **23** 542
[11] Bley M, Hurtado P I, Dzubiella J and Moncho-Jordá A 2022 *Soft Matter* **18** 397
[12] Liu Y, Zhu X, Wang Y, Chen Z and Huang F 2020 *Contrib. Plasma Phys.* **60** e201900190
[13] Wang J, Liu Y, Wang Y, Zhu W, Zhang W and Huang F 2021 *IEEE Trans. Plasma Sci.* **49** 1694
[14] Swope W C, Andersen H C, Berens P H and Wilson K R 1982 *J. Chem. Phys.* **76** 637
[15] Liu Y, Blosczyk N and Block D 2023 *Phys. Plasmas* **30** 043701
[16] Song Y L, Huang F, Chen Z Y, Liu Y H and Yu M Y 2016 *Phys. Lett. A* **380** 886
[17] Chen Z Y, Kong M H, Milošević M V and Wu Y C 2003 *Phys. Scr.* **67** 439
[18] Amiranashvili Sh G, Gusein-Zade N G and Tsytovich V N 2001 *Phys. Rev. E* **64** 016407
[19] Hou X N, Liu Y H, Huang F, Jiang S Z, Chen Z Y and Zhang R Y 2016 *Phys. Plasmas* **23** 093702
[20] Huang F, Liu Y H, Ye M F, Wang X J and Wang L 2010 *Chin. Phys. Lett.* **27** 115201
[21] Li W, Huang D, Wang K, Reichhardt C, Reichhardt C J O, Murillo M S and Feng Y 2018 *Phys. Rev. E* **98** 063203
[22] Wang K, Li W, Huang D, Reichhardt C, Reichhardt C J O, Murillo M S and Feng Y 2018 *Phys. Rev. E* **98** 063204
[23] Hou L J, Piel A and Shukla P K 2009 *Phys. Rev. Lett.* **102** 085002
[24] Huang D, Baggioli M, Lu S, Ma Z and Feng Y 2023 *Phys. Rev. Res.* **5** 013149
[25] Feng Y, Goree J and Liu B 2010 *Phys. Rev. Lett.* **104** 165003
[26] Feng Y, Goree J and Liu B 2012 *Phys. Rev. E* **86** 056403
[27] Liu B, Goree J, Pustylnik M Y, Thomas H M, Fortov V E, Lipaev A M, Usachev A D, Petrov O F, Zobnin A V and Thoma M H 2021 *IEEE Trans. Plasma Sci.* **49** 2972
[28] Rothermel H, Hagl T, Morfill G E, Thoma M H and Thomas H M 2002 *Phys. Rev. Lett.* **89** 175001
[29] Yang L, Schwabe M, Zhdanov S, Thomas H M, Lipaev A M, Molotkov V I, Fortov V E, Zhang J and Du C R 2017 *Europhys. Lett.* **117** 25001
[30] Durniak C, Samsonov D, Oxtoby N P, Ralph J F and Zhdanov S 2010 *IEEE Trans. Plasma Sci.* **38** 2412
[31] Zhdanov S, Nunomura S, Samsonov D and Morfill G 2003 *Phys. Rev. E* **68** 035401
[32] Edelsbrunner H and Seidel R 1985 *Proc. 1st Annu. Symp. Comput. Geom.* pp. 251–262
[33] Fortune S 1986 *Proc. 2nd Annu. Symp. Comput. Geom.* pp. 313–322
[34] Aurenhammer F and Klein R 2000 *Handbook of Computational Geometry* **5** 201
[35] Fortune S 2017 *Handbook of Discrete and Computational Geometry* (Chapman and Hall/CRC) pp. 705–721
[36] Brock J D 1992 *Bond-Orientational Order in Condensed Matter Systems* (Springer) pp. 1–31
[37] Woon W Y and Lin I 2004 *Phys. Rev. Lett.* **92** 065003
[38] Chan C L, Woon W Y and Lin I 2004 *Phys. Rev. Lett.* **93** 220602
[39] Ott T and Bonitz M 2009 *Phys. Rev. Lett.* **103** 195001
[40] Souzy M, Yin X, Villermaux E, Abid C and Metzger B 2015 *Phys. Fluids* **27** 045104
[41] Utter B and Behringer R P 2004 *Phys. Rev. E* **69** 031308
[42] Wong C S, Goree J, Haralson Z and Liu B 2018 *Nat. Phys.* **14** 21
[43] Pandey B P and Vranjes J 2005 *Phys. Scr.* **72** 247
[44] Wolf R A, Wan Y, Xing X, Zhang J C and Sazykin S 2009 *J. Geophys. Res. Space Phys.* **114** A09202
[45] Kaur P and Ganesh R 2019 *Phys. Rev. E* **100** 053201
[46] Popel S I 1998 *Phys. Scr.* **57** 272
[47] Wieben F and Block D 2019 *Phys. Rev. Lett.* **123** 225001